AGU PUBLICATIONS

Geophysical Research Letters

RESEARCH LETTER
10.1002/2017GL074368

Key Points:
- The 2016 seasonal velocity speedups of Zachariae and 79N are 14% and 11%, respectively, consistent with elsewhere on Greenland and are likely triggered by enhanced subglacial sliding due to surface melting
- The 79N speedup is unaffected by subglacial sticky spots and is incompatible with enhanced sliding along the sidewalls confining its floating tongue, whereas for Zachariae the ice mélange at its front might play an important role
- The 76 km long floating tongue of 79N provides, at most, only little resistance from its innermost part, and the remaining outer ~56–66 km could be lost without large consequences

Supporting Information:
- Supporting Information S1

Correspondence to:
N. M. Rathmann,
rathmann@nbi.ku.dk

Citation:
Rathmann, N. M., C. S. Hvidberg, A. M. Solgaard, A. Grinsted, G. H. Gudmundsson, P. L. Langen, K. P. Nielsen, and A. Kusk (2017), Highly temporally resolved response to seasonal surface melt of the Zachariae and 79N outlet glaciers in northeast Greenland, *Geophys. Res. Lett.*, *44*, 9805–9814, doi:10.1002/2017GL074368.

Received 3 JUN 2017
Accepted 20 AUG 2017
Accepted article online 24 AUG 2017
Published online 13 OCT 2017

Highly temporally resolved response to seasonal surface melt of the Zachariae and 79N outlet glaciers in northeast Greenland

N. M. Rathmann[1], C. S. Hvidberg[1], A. M. Solgaard[2], A. Grinsted[1], G. H. Gudmundsson[3], P. L. Langen[4], K. P. Nielsen[4], and A. Kusk[5]

[1]Center for Ice and Climate, Niels Bohr Institute, University of Copenhangen, Copenhagen, Denmark, [2]Geological Survey of Denmark and Greenland, Copenhagen, Denmark, [3]British Antarctic Survey, Cambridge, United Kingdom, [4]Danish Meteorological Institute, Copenhagen, Denmark, [5]National Space Institute, Technical University of Denmark (DTU), Lyngby, Denmark

Abstract The seasonal response to surface melting of the Northeast Greenland Ice Stream outlets, Zachariae and 79N, is investigated using new highly temporally resolved surface velocity maps for 2016 combined with numerical modeling. The seasonal speedup at 79N of 0.15 km/yr is suggested to be driven by a decrease in effective basal pressure induced by surface melting, whereas for Zachariae its 0.11 km/yr seasonal speedup correlates equally well with the breakup of its large ice mélange. We investigate the influence 76 km long floating tongue at 79N, finding it provides little resistance and that most of it could be lost without impacting the dynamics of the area. Furthermore, we show that reducing the slipperiness along the tongue-wall interfaces produces a velocity change spatially inconsistent with the observed seasonal speedup. Finally, we find that subglacial sticky spots such as bedrock bumps play a negligible role in the large-scale response to a seasonally enhanced basal slipperiness of the region.

Plain Language Summary The Northeast Greenland Ice Stream may potentially contribute significantly to near-term sea level rise and is one of the lesser studied Greenlandic systems, partly due to its remoteness. We present a new high temporally resolved velocity data set derived from Sentinel 1-A which allows capturing changes on a seasonal timescale, a feature which only the newest generation satellites now permit. We show how surface melting may be linked to the observed seasonal velocity changes, giving important insights into the possible future (range of) behavior and sensitivity of the ice stream outlets to atmospheric changes. In addition, we present a detailed study of possible moderating factors on the seasonal velocity response. In particular, we find that (i) the large ice mélange in front of the Zachariae outlet might be dampening the outlet's response, (ii) small-scale subglacial topographical bumps (sticky spots) exert very limited control on the flow, and (iii) the 76 km long floating tongue of the 79N outlet is largely a passive feature, suggesting that most of it (~80%) could be lost without effecting the outlet's contribution to near-term sea level rise. This has broad implications for assessing the future mass loss of ice sheets since it points to the importance of studying every major calving event individually.

1. Introduction

The Northeast Greenland Ice Stream (NEGIS) is a remarkable and rare dynamical flow feature of ice sheets. Being the only of its kind in Greenland, it extends more than 600 km into the interior of the ice sheet (Figure 1a, inset, colored contours) and terminates in three marine glaciers, 79N (NI), Zachariae (ZA), and Storstrømmen [*Fahnestock et al.*, 2001a; *Joughin et al.*, 2001]. The northernmost two, NI and ZA, drain approximately 198,380 km^2 (12%) of the ice sheet surface area (16% considering all three, dashed line in Figure 1, inset [*Zwally et al.*, 2012]), holding 1.1 m of sea level rise equivalent in their marine-based sector alone [*Morlighem et al.*, 2014; *Mouginot et al.*, 2015] (Figure 1b, blue contours).

Because of its unusual geometry and potentially large contribution to near-term sea level rise, NEGIS is being studied with increasing interest in order to quantify, and better understand, possible mass-flux drivers and responses to perturbations under the present and a warming climate. On one hand, numerical models used to quantify ice flow are increasingly attempting to resolve NEGIS as a coherent flow structure in large scale

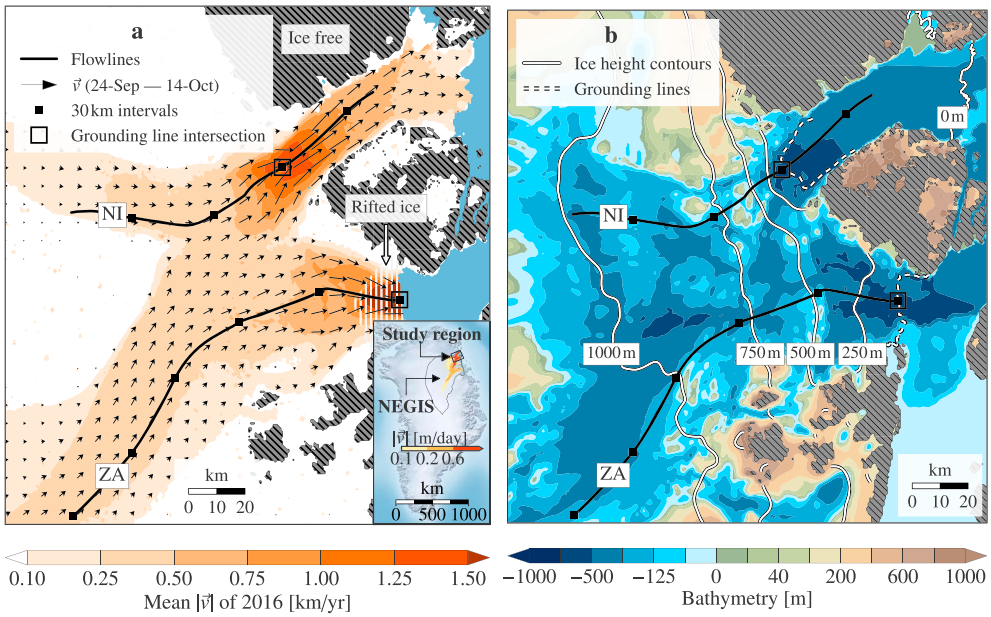

Figure 1. Ice surface velocities ($\vec{v}$), flow lines, and bed/surface topography of Zachariae (ZA) and 79N (NI) outlet glaciers. (a) Mean $|\vec{v}|$ of 2016 (colored contours), $\vec{v}$ (wherever $|\vec{v}|$>0.1 km/yr) between 24 September and 14 October 2016 (arrows), and ZA and NI flow lines (black lines). The inset shows the northeast Greenland ice stream (NEGIS) drainage area [*Zwally et al.*, 2012] (dashed black line) together with the NEGIS surface velocity wherever $|\vec{v}|$>0.1 m/d (colored contours). (b) Basal topography (colored contours) [*Bamber et al.*, 2001; *Morlighem et al.*, 2014], smoothed ice height contours (white lines) [*Howat et al.*, 2014], and ESA CCI 2016 grounding lines (dashed white lines) [*ENVEO*, 2016a] and calving fronts [*ENVEO*, 2016b]. Gray hatched regions mark ice-free surfaces in both panels.

(ice sheet wide) modeling [*Greve and Otsu*, 2007; *Seddik et al.*, 2012; *Greve and Herzfeld*, 2013; *Schlegel et al.*, 2013; *Ahlkrona et al.*, 2016], thereby allowing for insights into, e.g., the role played by basal friction and topography [*Joughin et al.*, 2001; *Greve and Otsu*, 2007; *Sergienko et al.*, 2014; *Schlegel et al.*, 2015; *Krabbendam*, 2016], the stationarity of its position [*Karlsson and Dahl-Jensen*, 2015], and the influence of external forcings on downstream mass fluxes [*Schlegel et al.*, 2015]. On the other hand, new observational data continues to shed light on otherwise unknown, or poorly understood, features of the flow, such as the geothermal hotspot suggested to initiate NEGIS by lubricating the bed [*Fahnestock et al.*, 2001b; *Layberry and Bamber*, 2001; *Bamber et al.*, 2013; *Christianson et al.*, 2014; *Keisling et al.*, 2014; *Rogozhina et al.*, 2016], dynamically induced mass losses by a multitude of external forcings [*Khan et al.*, 2014], the influence of sea ice and the warm regional ocean circulation around NI [*Thomsen et al.*, 1997; *Mayer et al.*, 2000; *Reeh et al.*, 2000, 2001], the complicated ice rheology near the upstream bounding shear margins [*Bell et al.*, 2014], and interannual surface velocities suggesting nontrivial, dissimilar behaviors of the two neighboring terminus glaciers, NI and ZA [*Mouginot et al.*, 2015].

In this work, we further investigate the *seasonal* behavior of the ZA and NI outlets by considering new high-temporal resolution surface velocity maps available every ~12–20 days throughout 2016, combined with atmospheric, subsurface, and ice flow modeling. Our aim is to put the observed interannual speedup of ZA and NI into a seasonal context and to investigate to what extent seasonal and interannual drivers are similar, which may help to better understand future changes.

2. Method and Results

Our analysis focuses on the observed 2016 seasonal behavior along the flow lines of ZA and NI (Figure 1). The dimensions of the region investigated were chosen based on the interferometric wide swath width of European Space Agency (ESA)'s Sentinel-1, which roughly overlaps with the domain considered by *Mouginot et al.* [2015]. We use ESA Sentinel-1 synthetic aperture radar (SAR) data from tracks 074, 170, and 112 with a 12 day repeat (24 day repeat in one case) between images to derive ice velocities. Data from these three tracks were combined to construct 28 surface ice velocity maps for 2016 of the ZI and NI area with best possible spatial coverage. The operational interferometric post processing (IPP) chain [*Dall et al.*, 2015], developed at the Technical University of Denmark (DTU) Space and upgraded with offset tracking for ESA's Climate

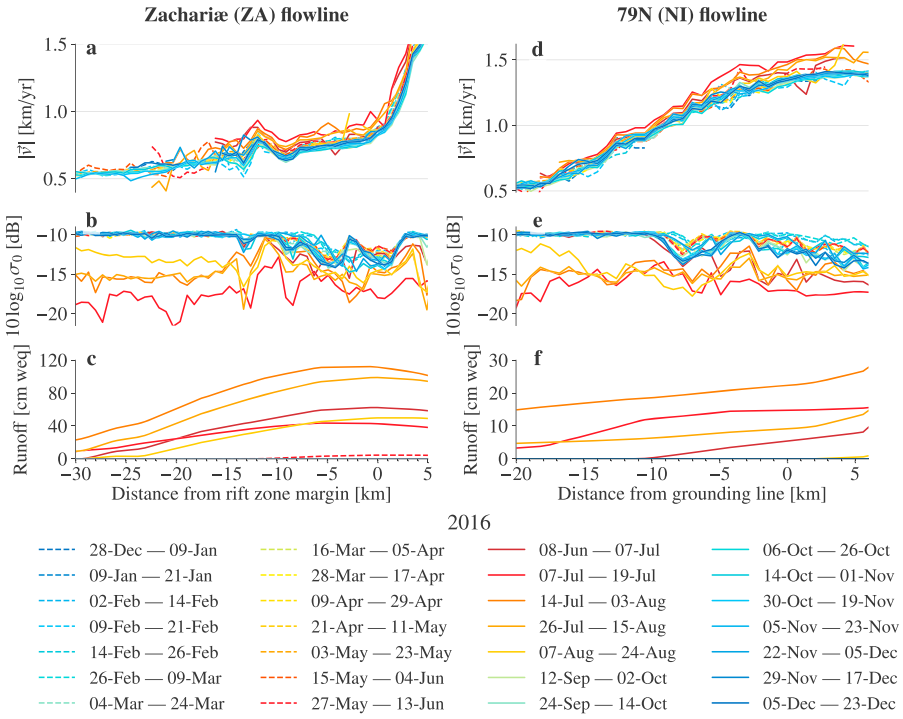

Figure 2. Flow line profiles along ZA and NI. (a and d) Ice surface speeds, $|\vec{v}|$. (b and e) Radar cross-section σ_0 (surface backscatter) from Sentinel-1A synthetic aperture radar (SAR) images [*Copernicus*, 2016] (high/low values are dry/wet surface conditions). (c and f) Simulated accumulated runoff estimates (between the legend periods) using the subsurface model by [*Langen et al.*, 2015, 2017].

Change Initiative (CCI) Greenland project, was employed to derive the surface movement using offset tracking [*Strozzi et al.*, 2002] assuming surface parallel flow using the digital elevation model from the greenland mapping project (GIMP DEM) by *Howat et al.* [2014, 2015]. The ice velocity data are freely available from www.promice.dk.

Figure 1a shows the 2016 mean surface velocity in colored contours based on the 28 velocity maps covering 2016, and Figure 1b shows the bounding geometry of the region based on basal topography by *Bamber et al.* [2001] and *Morlighem et al.* [2014], ice thicknesses from the GIMP DEM, and calving fronts and grounding lines by *ENVEO* [2016a, 2016b]. We note that the true ZA grounding line of 2016 is most likely located ~15 km upstream of the ESA grounding line, as suggested by the heavily rifted ice occurring on the remnant shelf after the recent collapse of its floating tongue (vertically white hatched area in Figure 1a, see the supporting information section S2).

These new highly temporally resolved surface velocity maps uniquely allow for detailed, remote process studies. The top panels in Figure 2 show the along-flow line velocity profiles of (a) ZA and (d) NI for selected, approximately evenly spaced, intervals of dates throughout 2016, ranging from winter (dashed blue) through summer (dashed/solid red) to winter (solid blue). At the ZA outlet, a seasonal speedup is initiated between 8 June and 7 July, reaching more than 15 km–30 km upstream from the rifted ice margin (supporting information section S2). After peaking with an increase of approximately 0.11 km/yr (14%) near the rifted ice margin, a return to the winter baseline occurs between 12 September to 2 October. For NI, the speedup, too, starts between 8 June to 7 July, peaks in 7–19 July with an increase of approximately 0.15 km/yr (11%) near the grounding line, and returns to its winter baseline between 7 and 24 August.

In regions of fast flowing ice, such as ice streams, the motion is generally attributed to a plug-like flow (constant velocity and strain rate throughout the thickness of the ice column) whereby the ice slides over the bed due to deformation of soft sedimentary substrate (till) or due to a low effective pressure in the subglacial drainage system, defined as the difference between the overburden and basal water pressure [*Rose*, 1979; *Alley et al.*, 1986; *Clarke*, 1987; *Macayeal et al.*, 1995; *Luthi et al.*, 2002]. While the far upstream part of NEGIS likely experiences a lowered effective pressure (permitting enhanced sliding) due to large basal melt

rates [*Fahnestock et al.*, 2001b; *Christianson et al.*, 2014; *Keisling et al.*, 2014], the basal state of the lower part is less known. It is, however, likely that the downstream basal environment is not water saturated in the sense that any additional water source could further enhance basal sliding. If so, it is plausible that the observed speedups are caused by seasonal surface melt penetrating through the ice and decreasing the effective pressure and/or lubricating the bed, as opposed to, e.g., ocean warming at the fronts suggested to trigger the observed decadal speedups [*Mouginot et al.*, 2015]. This mechanism has previously been suggested as a driver of seasonal speedups at different outlet glaciers by subglacial channels being flooded at the onset of the melt season, thereby increasing the basal water pressure leading to distributed drainage through interconnected cavities (effectively creating a small film of water lifting the ice from its substrate) [*Joughin et al.*, 2008a; *Stearns et al.*, 2008; *Schoof*, 2010; *Chandler et al.*, 2013; *Moon et al.*, 2014]. Later in the melt season when larger subglacial conduits (channels) effectively dominate the water transport, the water pressure drops (effective pressure increases) and the enhanced sliding ceases. This behavior has led to the suggestion that melt water variability, rather than the mean flux or total amount, plays an important role in seasonally enhanced sliding [*Bartholomaus et al.*, 2008; *Cuffey and Paterson*, 2010; *Schoof*, 2010].

To test this hypothesis at ZA and NI, surface backscatter (radar cross section, σ_0) from Sentinel-1A synthetic aperture radar (SAR) images [*Copernicus*, 2016] was investigated for signs of melting synchronous with the velocity speedups. Since SAR backscattering over snow covers arises from subsurface volume scatterers of snow/ice structures, such backscattering is sensitive to the wetness of the surface layer, which has previously successfully been used to identify surface melting over Greenland on diurnal and seasonal timescales [*Nghiem et al.*, 2001; *Steffen et al.*, 2004]. Figures 2b and 2e show that the backscatter along the two flow lines indeed drops synchronously with the speedups (high/low values indicating dry/wet conditions), suggesting the melt water quickly penetrates the ice (e.g., through crevasses or by hydraulic fracturing [*Fountain et al.*, 2005; *van der Veen*, 2007; *Bartholomaus et al.*, 2008; *Das et al.*, 2008]). Figure S1 in the supporting information further displays the spatial extent of the melting, indicating not only surface melting reaching far upstream but also a multitude of surface melt lakes, some as large as ≈5 km in diameter and rivers up to ≈20 km long, confirming the presence of large amounts of surface melt water. Note that the existence of large lakes could, potentially, delay the delivery of large volumes of water to the bed since filling and draining of lakes may be separated by several weeks.

To further quantify the amount of liquid water equivalent (weq) present, we invoke the firn (subsurface) model used in HIRHAM5 as documented by *Langen et al.*, 2015 [HIRHAM5, 2017] but used in an operational setup forced with 6-hourly surface energy fluxes and precipitation from the Danish Meteorological Institute's weather forecast model, HIRLAM 7.3 K05 [*Undén et al.*, 2002; *Rontu et al.*, 2009; *Kjellström et al.*, 2005]. The firn model allows the surface liquid water budget to be decomposed into components such as surface melt water runoff, retention in snow pack, refreezing, and more. The accumulated runoff along the two flow lines is shown in Figures 2c and 2f (accumulated over the time span indicated by the legends), suggesting poor retention in the firn and potentially large amounts of surface melt that could reach the bed.

The fact that similar velocity changes occur along ZA and NI with almost an order of magnitude more runoff along ZA compared to NI (on equal time intervals, Figures 2c and 2f) might suggest that melt water variability, and not the total amount, is driving the observed speedup. Claiming that melting is the driver alone, however, would be disregarding the possible seasonally dependant effects of the large ice mélange in front of ZA, the floating tongue of NI, and the differences in basal environment along ZA and NI which could, potentially, moderate their responses due to, e.g., sticky spots. If increased (upstream) basal lubrication is indeed causing the observed changes alone, one might expect the ice mélange, floating tongue, and potential sticky spots to exert only limited control over the velocity.

2.1. Role of the 79N Floating Tongue

To determine the influence of the 79N floating tongue, we further investigate if the tongue provides any resistance at the grounding line, and to what degree it might change during the seasonal speedup. Principally, such change could be caused either by a softening/warming of the fabric, thereby changing the internal stress configuration of the tongue, or by an enhanced sliding occurring along the tongue-wall interfaces. In the supporting information section S3, we show that derived strain rate maps indicate no seasonality, suggesting little internal stress redistribution over the season. Moreover, noting that the NI shear margins are relatively confined (Figure 3a), one might expect a weak coupling between the tongue and sidewalls. However, noting the upstream shear margin widths are similar, and that our estimates of slipperiness along the sidewalls

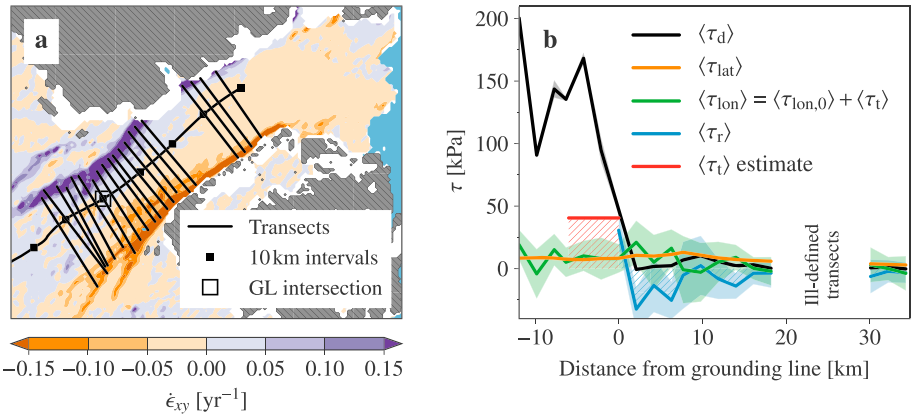

Figure 3. 79N stress budget derived from observations. (a) Strain rate field $\dot{\epsilon}_{xy}$ of 24 September and 14 October (in the local basis of the ground line transect) used to delineate transects; (b) transect-averaged stress components, where full lines are 2016 annual means and shades cover ±1 standard deviation.

are comparable to the subglacial values (supporting information section S4), we in the following give a more detailed account of the role played by the tongue.

We note, however, that floating tongues are unlikely to contribute to the stress budget of upstream grounded ice by actively providing resistance since (i) basal drag and lateral resistance from shear margins generally support grounded ice well, (ii) low-sloping equilibrium profiles are more likely to develop than tongues with frictionless bases holding back high-sloping grounded ice, and (iii) shear margins of sidewall-bounded tongues are likely weak (soft) because shearing tends to warm the ice, which, unlike for (unbounded) grounded ice shear margins, is not replaced with cold ice by cross-margin flow.

In section 2.1.1, we adopt the data-oriented approach by *Van Der Veen et al.* [2011] to show that even if the ice is assumed anchored to the sidewalls, the potential size (upper limit) of the resistive stress is indeed small compared to the total (driving) stress budget. Note that while this suggests the tongue is mostly a dynamically passive feature, it is not passive in the sense that removing the tongue would still produce a speedup because the sea water column alone can no longer balance the weight of the ice. Subsequently in section 2.1.2, we study the sensitivity of 79N to perturbations in basal slipperiness along the tongue-sidewall interfaces and over the remaining grounded ice using the numerical ice flow model Úa [*Gudmundsson et al.*, 2012], suggesting the seasonal speedup is likely related to upstream changes in basal slipperiness and not enhanced sidewall slipperiness.

2.1.1. Potential Resistance Provided by the 79N Tongue

In the *Van Der Veen et al.* [2011] approach, the sizes of the different stress components are estimated along the flow line by calculating their average values over transects locally perpendicular to the flow. These transects, which are picked at evenly spaced intervals (here $\Delta x = 2$ km), are delineated by their intersection with the ice stream shear margins, defined as the parallel belts of maxima and minima in the strain rate field $\dot{\epsilon}_{xy}$ (Figure 3a, orange/purple belts). Note that while transect orientations do not change much over the course of 2016, their widths (i.e., shear margin positions) do during the summer speedup, in part due to poorer spatial coverage, which is accommodated for in the following by calculating transect widths for each velocity map. Note also that x and y denote the local (transect-wise) along-flow and normal directions.

Assuming plug flow, a transect-wise stress balance on the grounded part of NI implies that the driving stress (τ_d) is balanced by flow-resisting stresses associated with lateral drag imposed by shear margins (τ_{lat}), along-flow longitudinal tension/compression (τ_{lon}), and basal drag (τ_b), that is

$$\tau_d = \tau_{lat} + \tau_{lon} + \tau_b \qquad \text{(grounded part)}. \tag{1}$$

The first three terms are defined as $\tau_d = -\rho g \overline{H \partial h/\partial x}$, $\tau_{lat} = 2B(H_N \dot{\epsilon}_{xy,N}^{1/n} - H_S \dot{\epsilon}_{xy,S}^{1/n})/W$, and $\tau_{lon} = -2B\overline{\partial (H \dot{\epsilon}_{xx}^{1/n})/\partial x}$, where $\overline{(\cdots)}$ denotes the transect average, $\rho = 917$ kg/m^3 the density of ice, $g = 9.8$ m/s the gravitational acceleration, H the ice thickness, h the surface height, W the transect width, and $n = 3$ is the Glen flow exponent. The flow parameter B was set to $B = A^{-1/n} = 275$ kPa/a^3 (A being the rate factor),

corresponding to an ice temperature of −5°C, assuming the ice is warmer than the mean surface air temperature, which in 2016 was −13°C between the NI grounding line and 20 km upstream (HIRLAM 7.3 K05 data). Finally, the subscripts in H_N and H_S denote point evaluations on the northern (N) and southern (S) shear margins respectively (similarly for $\dot{\epsilon}_{xy,N}$ and $\dot{\epsilon}_{xy,S}$).

Note that the quantity of interest here, the tongue's (resistive) contribution to the longitudinal stress field, hereafter referred to as τ_t, is not directly obtainable from the observed strain rates, $\dot{\epsilon}_{xx}$, since these reflect the influence of the net longitudinal stress, $\tau_{lon} = \tau_{lon,0} + \tau_t$, where $\tau_{lon,0}$ is the component associated with the local ice geometry.

For the floating tongue, however, there is no basal drag, and the stress balance becomes

$$\tau_d = \tau_{lat} + \tau_{lon} + \tau_r \qquad \text{(floating part)}, \tag{2}$$

where $\tau_d = -1/2\rho g(1-\rho/\rho_w)\overline{\partial H^2/\partial x}$, $\rho_w = 1027$ kg/m^3 being the density of sea water, and $\tau_r = \tau_d - \tau_{lat} - \tau_{lon}$ is the stress residual/imbalance, which is $\tau_r = 0$ along the buttressed part of the tongue and $\tau_r < 0$ along the part potentially contributing to resisting the upstream flow.

Figure 3b shows the 2016-averaged components (full lines) $\langle\tau_d\rangle$, $\langle\tau_{lat}\rangle$, $\langle\tau_{lon}\rangle$, and the residual $\langle\tau_r\rangle$, together with their standard deviation (filled colors). The figure indicates that (i) the residual, $\langle\tau_r\rangle$, is negative, suggesting the tongue may provide some resistance, but (ii) that resistance is predominately provided by the first 10–20 km of the tongue, after which $\langle\tau_r\rangle \approx 0$.

In order to estimate the size of τ_t, we note that the integrated stress residual (hatched blue in Figure 3b) must be balanced at the grounding line by the integral of τ_t from the grounding line and one coupling length upstream (hatched red in Figure 3b), here chosen as 10 grounding line ice thicknesses ($10H_{gl} = 6.0$ km), that is

$$\int_{0\text{km}}^{15\text{km}} \langle\tau_r\rangle \, dx = \int_{-10H_{gl}}^{0\text{km}} \langle\tau_t\rangle \, dx \approx 10H_{gl}\langle\tau_t\rangle. \tag{3}$$

Note that previous reports on coupling lengths suggest values between 7 and 15 ice thicknesses [*Howat et al.*, 2005, 2008; *Kamb and Echelmeyer*, 1986]. Assuming $\langle\tau_t\rangle$ to be evenly distributed over the coupling length, rightmost integral in equation (3) may be approximated accordingly, thus allowing for a low order estimation of $\langle\tau_t\rangle$ (red line in Figure 3b). In this case, the average ratio of (tongue) resistive stress to driving stress over the coupling length is $\langle\tau_t\rangle/\langle\tau_d\rangle^* = 34\%$, where $\langle\tau_d\rangle^* = (10H_{gl})^{-1}\int_{-10H_{gl}}^{0\text{km}}\langle\tau_d\rangle \, dx$. Note the above are upper estimates in the sense that the tongue might not be fully anchored to its sidewalls.

2.1.2. 79N Sensitivity to Tongue Length and Basal Slipperiness

In addition to estimating the potential resistive stress using the above data-oriented method, we also numerically consider the velocity response along 79N to changes in basal slipperiness and tongue length by using the finite-element ice flow model Úa [*Gudmundsson et al.*, 2012] based on the shallow shelf approximation.

In section S4 in the supporting information, we use Úa for two separate sets of perturbation experiments whereby the basal slipperiness and tongue length are covaried: in the first set the slipperiness along the tongue-sidewall interfaces is uniformly perturbed relative to the slipperiness inverted from winter time velocities, whereas in the second set the slipperiness under the remaining (upstream) grounded ice is uniformly perturbed. Considering both sets of perturbations thus allows us to test the hypothesis that seasonal changes are caused by an upstream increase in basal slipperiness (melt-induced enhanced sliding) rather than e.g., downstream enhanced sliding along the sidewalls of the tongue.

The results suggest that once the tongue is less than 15 km long, the grounding line velocity becomes very sensitive to any further decrease in tongue length, which is in agreement with the observational based analysis in section 2.1.1, suggesting the innermost part might provide resistance. Note, however, that some speedup is to be expected even without a tongue providing resistance because of the large thickness changes that occur over the innermost part — cutting off the tongue there produces a force imbalance since the weight of the removed tongue is replaced by the weight of a smaller column of sea water.

Considering the flow line response to uniform slipperiness perturbations over the grounded ice, the model suggests that a ∼20% increase in upstream slipperiness is enough to reproduce both the amplitude and spatial extent of the seasonal velocity change. Moreover, we find that enhanced sliding along the tongue-sidewall margins alone gives rise to velocity changes only locally over the tongue. Thus, it seems unlikely the tongue

plays a role in the seasonal speedup in the sense that increased sliding along the tongue-sidewall interface cannot account for the full spatial extent of the observed seasonality. Instead, the speedup magnitude and spatial extent seems consistent with a ~20% increase in upstream basal slipperiness.

2.2. Role of the Zachariae Ice Mélange

In the supporting information, we further investigate the influence and timing of the Zachariae ice mélange breakup. By defining the mélange as being mobilized/broken-up by the loss of surface feature correlation between consecutive SAR images, indicating fast moving ice escaping the feature tracking window and/or surface features being degraded due to melting, we find that the break up coincides with the onset of surface melting upstream of the rifted zone, approximately 8 June. Note that because of the large height differences of around 250 m – 500 m between the rifted front and the upstream part, this needed not be so. The two events coinciding does, unfortunately, not allow us to discern whether the ice mélange is in fact strong enough to trigger upstream changes upon disintegration, or if surface melting is responsible. Nonetheless, Zachariae is potentially an important case for further understanding the relative roles played by ice mélanges and surface melting/basal lubrication in seasonal changes, one where mélange modeling and multi-year seasonal velocity datasets may prove useful.

2.3. Role of Potential Subglacial Sticky Spots

Localized patches of basal friction, or "sticky spots," have previously been suggested to play an important role in the dynamics of ice streams [*Kamb*, 1991; *Alley*, 1993; *Stokes et al.*, 2007]. Generally caused by bedrock bumps, till-free areas, or subglacial meltwater frozen to the bed, sticky spots may help to stabilize ice streams [*Kamb*, 1991; *Stokes et al.*, 2007]. Because bedrock bumps are regarded as likely sources of sticky spots [*Alley*, 1993] and are possibly influential under active ice streams [*Stokes et al.*, 2007], we further investigate in supporting information section S4.2 their potential role in moderating the seasonal velocity changes observed along ZA and NI.

Noting that the area along ZA with the greatest seasonal speedup is deeper, and likely weaker, than further upstream close to a couple of bedrock bumps, one might suspect the large number of bedrock bumps along NI to be especially influential. To determine their influence, we perform two sets of slipperiness perturbation experiments using Úa whereby (i) the slipperiness is varied for all grounded ice except over small-scale bedrock bumps (defined as bumps being taller than sea level) and (ii) the slipperiness is varied for all grounded ice in addition to bedrock bumps being flattened (artificially set to sea level height). We find that while the influence of bedrock bumps on the velocity field is small in magnitude and spatially local for both NI and ZA (not shown for latter), the details of the subglacial environment potentially exert a greater control on the seasonal velocity response compared to e.g., changes in slipperiness along the tongue-sidewall interfaces.

3. Discussion and Conclusions

Glaciers that discharge into the ocean are potentially large contributors to the uncertainty of sea level rise predictions of the near future. In particular, glaciers with floating tongues add to this uncertainty by their tongues possibly acting as a downstream plug holding back the flow of ice. This underlines the need for understanding the processes leading to the breaking up of floating tongues — be it by mechanical failure due to changes in the stress configuration, subsurface hot water plumes destabilizing the tongue, related to calving by surface melting filling up crevasses, or the ice mélange breaking up because of wind stresses. While there has been some debate over the driving mechanism behind the sudden doubling in ice discharge of Jakobshavn Isbræ coincident with the collapse of its floating tongue in 1998 [*Truffer and Echelmeyer*, 2003; *Joughin et al.*, 2008b; *Holland et al.*, 2008; *Van Der Veen et al.*, 2011], it stands, together with the recent large calving event at the Larsen C ice shelf, as important examples of the need to understand the processes governing the stability of floating tongues/shelves and whether they provide any resistance.

In this work, we found that the 76 km long floating tongue of 79N might provide some (small) resistance from the innermost 15 km, suggesting a greater speedup may follow a potential collapse than otherwise expected if it were just buttressed (albeit the resistance is small). This, we argue, emphasizes the need to consider the consequences of calving events on an individual basis. In the light of the results presented here, it seems important to understand the structural integrity of the 79N tongue to, e.g., the reported increasing surrounding mean ocean temperature over the last decade [*Mouginot et al.*, 2015]. In this context, we propose

that high temporally resolved velocity data sets might provide unique opportunities to understand the strength and durability of floating tongues (and their upstream systems) when exposed to changes in external forcings over long time scales by investigating their response to forcings on a seasonal time scale, such as attempted here.

In summary we presented a highly temporally resolved velocity data set derived from Sentinel-1A SAR imagery allowing for insights into the seasonal behavior and drivers of the Zachariae (ZA) and 79N (NI) outlet glaciers in northeast Greenland. We showed that extensive surface melt is present over ZA and NI, both area wise and in terms of water equivalent, by combining SAR images with a numerical firn (subsurface) model to quantify the seasonal runoff. In particular, we suggest that the observed speedups during the summer of 2016 of approximately 0.15 km/yr along NI is driven by surface melt water penetrating the ice and lubricating the bed (decreasing the effective basal pressure), whereas the 0.11 km/yr speedup along ZA correlates equally well with both the onset of surface melting and the breakup of its large ice mélange, making it less clear whether the ice mélange is in fact strong enough to induce the observed seasonal changes upon break up.

By decomposing the near-terminus stress budget of NI, we find the potential resistance provided by the floating tongue is at most on the order of 34% of the near-terminus stress budget (assuming the tongue is actually anchored to the wall) and is constant across season, suggesting it is unlikely that the tongue moderates the seasonal response much. By covarying the basal slipperiness and tongue length using the numerical ice flow model Úa, we furthermore found (i) that the outermost ~56–66 km of the tongue can be removed without making NI unstable, (ii) that only an upstream increase in basal slipperiness of the grounded ice can induce a change in the velocity field spatially consistent with the observed seasonal speedup (as opposed to, e.g., enhanced sliding along the tongue-sidewall interfaces), and (iii) that subglacial sticky spots, such as small-scale bedrock bumps, seem only to induce velocity changes small in magnitude and spatially local for both NI and ZA, thus probably not providing large-scale moderation of the observed seasonal response.

Acknowledgments
We wish to express our sincere thanks to two anonymous reviewers for valuable comments that helped greatly improve this manuscript. The research leading to these results has received funding from the European Research Council under the European Community's Seventh Framework Programme (FP7/2007-2013)/ERC grant agreement 610055 as part of the ice2ice project and from the Villum Investigator Project IceFlow. Ice velocity maps were produced from ESA Sentinel-1 remote sensing data as part the Programme for Monitoring of the Greenland Ice Sheet (PROMICE) and the ESA Greenland Ice Sheet Climate Change Initiative and were provided by the Geological Survey of Denmark and Greenland (GEUS) (freely available at www.promice.dk). Finally, we wish to acknowledge the important contribution made during the ice2ice bootcamp 2017 to section 2.1.1 by Faezeh M. Nick, Iben Koldtoft, Benjamin Keisling, Silje Smith-Johnsen, and Andreas Plach.

References

Ahlkrona, J., P. Lötstedt, N. Kirchner, and T. Zwinger (2016), Dynamically coupling the non-linear stokes equations with the shallow ice approximation in glaciology: Description and first applications of the ISCAL method, *J. Comput. Phys.*, *308*, 1–19.
Alley, R. B. (1993), In search of ice-stream sticky spots, *J. Glaciol.*, *39*(133), 447–454.
Alley, R. B., D. D. Blankenship, C. R. Bentley, and S. Rooney (1986), Deformation of till beneath ice stream B, West Antarctica, *Nature*, *322*(6074), 57–59.
Bamber, J. L., R. L. Layberry, and S. Gogineni (2001), A new ice thickness and bed data set for the Greenland ice sheet: 1. Measurement, data reduction, and errors, *J. Geophys. Res.*, *106*(D24), 33,773—33,780, doi:10.1029/2001JD900054.
Bamber, J. L., M. J. Siegert, J. A. Griggs, S. J. Marshall, and G. Spada (2013), Paleofluvial mega-canyon beneath the central Greenland ice sheet, *Science*, *341*(6149), 997–999.
Bartholomaus, T. C., R. S. Anderson, and S. P. Anderson (2008), Response of glacier basal motion to transient water storage, *Nat. Geosci.*, *1*(1), 33–37.
Bell, R., K. Tinto, I. Das, M. Wolovick, W. Chu, T. Creyts, N. Frearson, A. Abdi, and J. Paden (2014), Deformation, warming and softening of Greenland's ice by refreezing meltwater, *Nat. Geosci.*, *7*, 497–502.
Chandler, D. et al. (2013), Evolution of the subglacial drainage system beneath the Greenland ice sheet revealed by tracers, *Nat. Geosci.*, *6*(3), 195–198.
Christianson, K., L. E. Peters, R. B. Alley, S. Anandakrishnan, R. W. Jacobel, K. L. Riverman, A. Muto, and B. A. Keisling (2014), Dilatant till facilitates ice-stream flow in northeast Greenland, *Earth Planet. Sci. Lett.*, *401*, 57–69.
Clarke, G. K. (1987), Fast glacier flow: Ice streams, surging, and tidewater glaciers, *J. Geophys. Res.*, *92*(B9), 8835–8841.
Copernicus (2016), Copernicus sentinel data [2016]. [Available at https://scihub.copernicus.eu/.]
Cuffey, K. M., and W. S. B. Paterson (2010), *The Physics of Glaciers*, Acad. Press, New York.
Dall, J., A. Kusk, U. Nielsen, and J. P. Merryman Boncori (2015), Ice velocity mapping using tops sar data and offset tracking, in *Proceedings of 9th International Workshop Fringe 2015*, vol. 731, edited by L. Ouwehand, p. 14, ESA-SP, Frascati, Italy.
Das, S. B., I. Joughin, M. D. Behn, I. M. Howat, M. A. King, D. Lizarralde, and M. P. Bhatia (2008), Fracture propagation to the base of the Greenland ice sheet during supraglacial lake drainage, *Science*, *320*(5877), 778–781.
ENVEO (2016a), ENVEO/ESA Greenland Icesheet CCI, grounding lines from SAR interferometry. [Available at http://cryoportal.enveo.at/.]
ENVEO (2016b), ENVEO/ESA Greenland Icesheet CCI, calving frontline locations. [Available at http://cryoportal. enveo.at/.]
Fahnestock, M., I. Joughin, T. Scambos, R. Kwok, W. Krabill, and S. Gogineni (2001a), Ice-stream-related patterns of ice flow in the interior of northeast Greenland, *J. Geophys. Res.*, *106*(D24), 34,035–34,045, doi:10.1029/2001JD900194.
Fahnestock, M., W. Abdalati, I. Joughin, J. Brozena, and P. Gogineni (2001b), High geothermal heat flow, basal melt, and the origin of rapid ice flow in central Greenland, *Science*, *294*(5550), 2338–2342.
Fountain, A. G., R. W. Jacobel, R. Schlichting, and P. Jansson (2005), Fractures as the main pathways of water flow in temperate glaciers, *Nature*, *433*(7026), 618–621.
Greve, R., and U. C. Herzfeld (2013), Resolution of ice streams and outlet glaciers in large-scale simulations of the Greenland Ice Sheet, *Ann. Glaciol.*, *54*(63), 209–220.
Greve, R., and S. Otsu (2007), The effect of the north-east ice stream on the Greenland Ice Sheet in changing climates, *Cryosphere Discuss.*, *1*(1), 41–76.
Gudmundsson, G. H., J. Krug, G. Durand, L. Favier, and O. Gagliardini (2012), The stability of grounding lines on retrograde slopes, *Cryosphere*, *6*(6), 1497–1505, doi:10.5194/tc-6-1497-2012.

Holland, D. M., R. H. Thomas, B. De Young, M. H. Ribergaard, and B. Lyberth (2008), Acceleration of jakobshavn isbrae triggered by warm subsurface ocean waters, *Nat. Geosci.*, *1*(10), 659.
Howat, I. M., I. Joughin, S. Tulaczyk, and S. Gogineni (2005), Rapid retreat and acceleration of Helheim Glacier, east Greenland, *Geophys. Res. Lett.*, *32*, L22502, doi:10.1029/2005GL024737.
Howat, I. M., I. Joughin, M. Fahnestock, B. E. Smith, and T. A. Scambos (2008), Synchronous retreat and acceleration of southeast Greenland outlet glaciers 2000–06: Ice dynamics and coupling to climate, *J. Glaciol.*, *54*(187), 646–660.
Howat, I. M., A. Negrete, and B. E. Smith (2014), The Greenland Ice Mapping Project (GIMP) land classification and surface elevation data sets, *Cryosphere*, *8*(4), 1509–1518, doi:10.5194/tc-8-1509-2014.
Howat, I. M., A. Negrete, and B. E. Smith (2015), Measures Greenland Ice Mapping Project (GIMP) digital elevation model, version 1, *Cryosphere*, *8*, 1509–1518, doi:10.5067/NV34YUIXLP9W.
Joughin, I., M. Fahnestock, D. MacAyeal, J. L. Bamber, and P. Gogineni (2001), Observation and analysis of ice flow in the largest Greenland ice stream, *J. Geophys. Res.*, *106*(D24), 34,021–34,034, doi:10.1029/2001JD900087.
Joughin, I., S. B. Das, M. A. King, B. E. Smith, I. M. Howat, and T. Moon (2008a), Seasonal speedup along the western flank of the Greenland Ice Sheet, *Science*, *320*(5877), 781–783.
Joughin, I., I. M. Howat, M. Fahnestock, B. Smith, W. Krabill, R. B. Alley, H. Stern, and M. Truffer (2008b), Continued evolution of Jakobshavn Isbrae following its rapid speedup, *J. Geophys. Res.*, *113*, F04006, doi:10.1029/2008JF001023.
Kamb, B. (1991), Rheological nonlinearity and flow instability in the deforming bed mechanism of ice stream motion, *J. Geophys. Res.*, *96*(B10), 16,585–16,595.
Kamb, B., and K. A. Echelmeyer (1986), Stress-gradient coupling in glacier flow: IV. Effects of the "T" term, *J. Glaciol.*, *32*(112), 342–349.
Karlsson, N., and D. Dahl-Jensen (2015), Response of the large-scale subglacial drainage system of northeast Greenland to surface elevation changes, *Cryosphere*, *9*(4), 1465–1479.
Keisling, B. A., K. Christianson, R. B. Alley, L. E. Peters, J. E. Christian, S. Anandakrishnan, K. L. Riverman, A. Muto, and R. W. Jacobel (2014), Basal conditions and ice dynamics inferred from radar-derived internal stratigraphy of the northeast Greenland ice stream, *Ann. Glaciol.*, *55*(67), 127–137.
Khan, S. A. et al. (2014), Sustained mass loss of the northeast Greenland ice sheet triggered by regional warming, *Nat. Clim. Change*, *4*(4), 292–299.
Kjellström, E. et al. (2005), A 140-year simulation of european climate with the new version of the rossby centre regional atmospheric climate model (RCA3), in *SMHI Reports Meteorology and Climatology No. 108*, 54 pp., SMHI, SE-60176, Norrköping, Sweden.
Krabbendam, M. (2016), Sliding of temperate basal ice on a rough, hard bed: creep mechanisms, pressure melting, and implications for ice streaming, *Cryosphere*, *10*(5), 1915–1932.
Langen, P., et al. (2015), Quantifying energy and mass fluxes controlling Godthåbsfjord freshwater input in a 5-km simulation (1991–2012), *J. Clim.*, *28*(9), 3694–3713.
Langen, P. L., R. S. Fausto, B. Vandecrux, R. H. Mottram, and J. E. Box (2017), Liquid water flow and retention on the Greenland ice sheet in the regional climate model HIRHAM5: Local and large-scale impacts, *Front. Earth. Sci.*, *4*, 110.
Layberry, R., and J. Bamber (2001), A new ice thickness and bed data set for the Greenland ice sheet: 2. Relationship between dynamics and basal topography, *J. Geophys. Res.*, *106*(D24), 33,781—33,788.
Luthi, M., M. Funk, A. Iken, S. Gogineni, and M. Truffer (2002), Merchanisms of fast flow in Jakobshavn Isbrae, West Greenland: Part III. Measurements of ice deformation, temperature and cross-borehole conductivity in boreholes to the bedrock, *J. Glaciol.*, *48*(162), 369–385.
Macayeal, D. R., R. A. Bindschadler, and T. A. Scambos (1995), Basal friction of ice stream E, West Antarctica, *J. Glaciol.*, *41*(138), 247–262.
Mayer, C., N. Reeh, F. Jung-Rothenhäusler, P. Huybrechts, and H. Oerter (2000), The subglacial cavity and implied dynamics under Nioghalvfjerdsfjorden Glacier, NE-Greenland, *Geophys. Res. Lett.*, *27*(15), 2289–2292.
Moon, T., I. Joughin, B. Smith, M. R. Broeke, W. J. Berg, B. Noël, and M. Usher (2014), Distinct patterns of seasonal Greenland glacier velocity, *Geophys. Res. Lett.*, *41*(20), 7209—7216, doi:10.1002/2014GL061836.
Morlighem, M., E. Rignot, J. Mouginot, H. Seroussi, and E. Larour (2014), Deeply incised submarine glacial valleys beneath the Greenland ice sheet, *Nat. Geosci.*, *7*(6), 418–422, doi:10.1038/ngeo2167.
Mouginot, J., E. Rignot, B. Scheuchl, I. Fenty, A. Khazendar, M. Morlighem, A. Buzzi, and J. Paden (2015), Fast retreat of Zachariæ Isstrøm, northeast Greenland, *Science*, *350*(6266), 1357–1361.
Nghiem, S., K. Steffen, R. Kwok, and W.-Y. Tsai (2001), Detection of snowmelt regions on the Greenland ice sheet using diurnal backscatter change, *J. Glaciol.*, *47*(159), 539–547.
Reeh, N., C. Mayer, O. B. Olesen, E. L. Christensen, and H. H. Thomsen (2000), Tidal movement of Nioghalvfjerdsfjorden glacier, northeast Greenland: Observations and modelling, *Ann. Glaciol.*, *31*(1), 111–117.
Reeh, N., H. H. Thomsen, A. K. Higgins, and A. Weidick (2001), Sea ice and the stability of north and northeast Greenland floating glaciers, *Ann. Glaciol.*, *33*(1), 474–480.
Rogozhina, I. et al. (2016), Melting at the base of the Greenland ice sheet explained by Iceland hotspot history, *Nat. Geosci.*, *9*, 366–369, doi:10.1038/ngeo2689.
Rontu, L., F. Obleitner, S. Gollvik, C. Zingerle, and S. Tijm (2009), HIRLAM experiments on surface energy balance across Vatnajökull, Iceland, *Meteorol. Atmos. Phys.*, *103*(1), 67–77.
Rose, K. (1979), Characteristics of ice flow in Marie Byrd Land, Antarctica, *J. Glaciol.*, *24*(90), 63–75.
Schlegel, N., E. Larour, H. Seroussi, M. Morlighem, and J. Box (2013), Decadal-scale sensitivity of northeast Greenland ice flow to errors in surface mass balance using ISSM, *J. Geophys. Res. Earth Surf.*, *118*, 667–680, doi:10.1002/jgrf.20062.
Schlegel, N.-J., E. Larour, H. Seroussi, M. Morlighem, and J. Box (2015), Ice discharge uncertainties in northeast Greenland from boundary conditions and climate forcing of an ice flow model, *J. Geophys. Res. Earth Surf.*, *120*, 29–54, doi:10.1002/2014JF003359.
Schoof, C. (2010), Ice-sheet acceleration driven by melt supply variability, *Nature*, *468*(7325), 803–806.
Seddik, H., R. Greve, T. Zwinger, F. Gillet-Chaulet, and O. Gagliardini (2012), Simulations of the Greenland ice sheet 100 years into the future with the full Stokes model Elmer/Ice, *J. Glaciol.*, *58*(209), 427–440.
Sergienko, O., T. T. Creyts, and R. Hindmarsh (2014), Similarity of organized patterns in driving and basal stresses of Antarctic and Greenland ice sheets beneath extensive areas of basal sliding, *Geophys. Res. Lett.*, *41*, 3925–3932, doi:10.7916/D85X28CW.
Stearns, L. A., B. E. Smith, and G. S. Hamilton (2008), Increased flow speed on a large East Antarctic outlet glacier caused by subglacial floods, *Nat. Geosci.*, *1*(12), 827–831.
Steffen, K., S. Nghiem, R. Huff, and G. Neumann (2004), The melt anomaly of 2002 on the Greenland ice sheet from active and passive microwave satellite observations, *Geophys. Res. Lett.*, *31*, L20402, doi:10.1029/2004GL020444.

Stokes, C. R., C. D. Clark, O. B. Lian, and S. Tulaczyk (2007), Ice stream sticky spots: A review of their identification and influence beneath contemporary and palaeo-ice streams, *Earth Sci. Rev.*, *81*(3), 217–249.

Strozzi, T., A. Luckman, T. Murray, U. Wegmuller, and C. L. Werner (2002), Glacier motion estimation using SAR offset-tracking procedures, *IEEE Trans. Geosci. Remote Sens.*, *40*(11), 2384–2391.

Thomsen, H. H., N. Reeh, O. B. Olesen, C. E. Bøggild, W. Starzer, A. Weidick, and A. K. Higgins (1997), The Nioghalvfjerdsfjorden glacier project, North-East Greenland: A study of ice sheet response to climatic change, *Geol. Surv. Den. Greenl.*, *176*, 95–103.

Truffer, M., and K. A. Echelmeyer (2003), Of isbrae and ice streams, *Ann. Glaciol.*, *36*(1), 66–72.

Undén, P., L. Rontu, H. Järvinen, P. Lynch, and J. Calvo (2002), The HIRLAM-5 scientific documentation. HIRLAM-5 project, c/o per undén SMHI, s-601 76 Norrköping, Sweden. [Available at http://hirlam.org.]

van der Veen, C. J. (2007), Fracture propagation as means of rapidly transferring surface meltwater to the base of glaciers, *Geophys. Res. Lett.*, *34*, L01501, doi:10.1029/2006GL028385.

Van Der Veen, C. J., J. Plummer, and L. Stearns (2011), Controls on the recent speed-up of Jakobshavn Isbræ, West Greenland, *J. Glaciol.*, *57*(204), 770–782.

Zwally, H. J., M. B. Giovinetto, M. A. Beckley, and J. L. Saba (2012), Antarctic and Greenland drainage systems: GSFC Cryospheric Sciences Laboratory. [Available at http://icesat4.gsfc.nasa.gov/cryo_data/ant_grn_drainage_systems.php.]